

© 2016 IEEE. Personal use of this material is permitted. Permission from IEEE must be obtained for all other uses, in any current or future media, including reprinting/republishing this material for advertising or promotional purposes, creating new collective works, for resale or redistribution to servers or lists, or reuse of any copyrighted component of this work in other works.

E. M. Bates, W. J. Birmingham and C. Romero-Talamás, "Design Optimization of Nested Bitter Magnets," in IEEE Transactions on Magnetics, vol. 53, no. 3, pp. 1-10, March 2017, Art no. 7200310, doi: 10.1109/TMAG.2016.2645158.

<http://dx.doi.org/10.1109/TMAG.2016.2645158>

Access to this work was provided by the University of Maryland, Baltimore County (UMBC) ScholarWorks@UMBC digital repository on the Maryland Shared Open Access (MD-SOAR) platform.

**Please provide feedback**

Please support the ScholarWorks@UMBC repository by emailing [scholarworks-group@umbc.edu](mailto:scholarworks-group@umbc.edu) and telling us what having access to this work means to you and why it's important to you. Thank you.

# Design Optimization of Nested Bitter Magnets

Evan M. Bates<sup>1</sup>, William J. Birmingham<sup>1</sup>, Carlos A. Romero-Talamás<sup>1</sup>

<sup>1</sup>Dusty Plasma Laboratory, Department of Mechanical Engineering,  
University of Maryland Baltimore County, Baltimore, Maryland 21250

An optimization technique that utilizes a Genetic Algorithm (GA) is used to minimize the electrical power produced by the conducting disks in resistive Bitter magnets. The resulting values from the optimization give the conditional design parameters necessary for a preliminary magnet design. This precursor design method can be employed for either split or single solenoid nested designs. This method is used to design a 10T, 10 second magnet at the University of Maryland, Baltimore County for plasma physics research. The design parameters from the optimization are used to generate computer-aided design (CAD) models that are examined with finite element analysis (FEA) software to verify safety and performance of the design. The magnet design then progresses to a series of thermal and mechanical tests to ensure safe operating conditions.

**Index Terms**—Water cooled resistive Bitter magnet, Genetic algorithm optimization, Analytic magnetic field Solver, Preliminary electromagnet designing, FEA analysis

## I. INTRODUCTION

A Custom high field magnet is being designed at the University of Maryland, Baltimore County (UMBC) for magnetized dusty plasma experiments [1]. The use of magnets in experiments has proven to be highly valuable in numerous fields of research. In particular, accessibility to high magnetic fields is considered the next frontier for research in complex (dusty) plasmas [2]. Magnetic fields lead to charged particle gyration perpendicular to the magnetic field with a gyro-radius (also called Larmor radius) defined as  $r_L = \frac{v_{\perp}}{\omega_c}$ , where  $v_{\perp}$  is the particle's velocity perpendicular to the magnetic field and  $\omega_c$  is the angular frequency of the particle gyrating in the field. Until now, experiments that also include electric fields perpendicular to the magnetic field, have magnetized the electrons and ions, but not the dust of size bigger than a few hundred nanometers, as the Larmor radius of the latter has not been sufficiently small compared to reported experimental devices. It is of interest to investigate fundamental properties of materials using dusty plasmas as atomistic models to gain first principles understanding of viscosity in sheared rotating flows, the physics of friction using dusty plasma crystals including thermal and mechanical properties of such crystals, and migration of dust in high-temperature magnetized plasma confinement devices.

In order to magnetize dust particles that are big enough for diagnostics to follow them individually, a magnetic field of amplitude 10 Tesla (T) is needed for at least 10 seconds. To achieve this, a water cooled Bitter-type electromagnet is being designed. This type of magnet was first created by Francis Bitter in the 1930s to solve the problem of ohmic heating associated with high currents [3]. The magnet consists of copper-alloy plate conductors with cooling holes, separated by insulating plates. Current travels through the helically-stacked conductors to create an axial uniform field inside the bore. Cooling liquid passes through holes in the plates to dissipate heat. The Bitter magnet design has been greatly improved upon within the last couple decades. One of the

most notable advancements in Bitter magnet design was that of the *Florida – Bitter* magnet [6], [7]. Researchers have reached steady DC (Direct Current) fields of 33T without superconducting coils, and more recently, continuous fields of a record breaking 37.5T at NHML (Nijmegen High Field Magnet Laboratory) [4], [5]. Our proposed magnetized dusty plasma experiments would benefit from the highest achievable magnetic fields, such as 33T and 37.5T; however, many high field resistive magnets are too small to accommodate the scale of a practical dusty plasma experiment. The 33T and 37.5T magnets both have a 32mm Type II bore (cylindrical opening in Fig. 1). There is no magnet currently that can accommodate a 10T DC field with a minimum bore of 160mm for our custom magnetized dusty plasma experiments.

This paper will outline the optimization of Bitter magnets for dusty plasma research where a custom built vacuum chamber of 160mm (6.3”) diameter will be immersed in the uniform magnetic field. The bore of the magnet is the experimental volume, and details of experiment setup will be outlined elsewhere. We have explored two different design concepts for our research: split and solenoid Bitter magnets, both including up to three nested coils, two examples are seen in Fig. 1. The nested split magnet is symmetric about the center axis and allows for more optical access to a vacuum chamber at the expense of electric current needed to reach the necessary fields. The nested solenoid provides a substantial drop in current, but optical access to our experiments becomes more challenging.

The goal of the optimization of Type I (split) and Type II (solenoid) magnets is a cost efficient design of a uniform magnetic field of at least 10T. The optimization outputs key features of the magnet, but does not consider mechanical stresses nor does it account for the current density profile effect by the placement of cooling and tierod holes. This optimization serves as a preliminary design which can be iterated based on feedback from mechanical design considerations. Parameters from this design are used to evaluate the inductance, forces and stresses on an entire system under development at UMBC. The finished system will be reported

Corresponding author: Evan M. Bates (email: evbates1@umbc.edu).

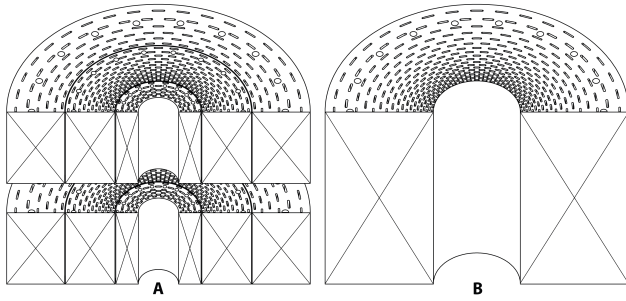


Fig. 1. (A) Type - I Magnet,  $\alpha = 3$ . The experiment volume is the horizontal space between the nested coils (B) Type - II Magnet  $\alpha = 1$ . In this case the experiment volume is the cylindrical space inside the coil. For both cases  $\alpha$  is the number of coils nested.

elsewhere.

## II. ELECTRICITY & MAGNETISM MATHEMATICAL FOUNDATION

The formulation of this optimization problem requires the derivation of a model that allows the calculation of the magnetic field and electrical power based on design parameters described here. The model is simplified to allow for fast computations during parameter exploration, yet precise enough to only have a small percentage difference with respect to finite element analysis, as shown below.

### A. Electrical Power

An efficient magnet is one that maximizes the magnetic field amplitude at the lowest possible power [8]. We want to minimize the amount of ohmic heat that needs to be dissipated through water cooling, but will not surpass the yield strength of the conducting material that will be used. If there is too much heat and the yield strength of the material is reached, the system will be compromised and the Lorentz force, given by  $\mathbf{J} \times \mathbf{B}$ , where  $\mathbf{J}$  is the current density and  $\mathbf{B}$  the magnetic field, will cause the magnet to fail catastrophically. Power for a nested system as seen in Fig. 1a is given by Ohm's law, where:

$$Power = \sum_{k=1}^{\alpha} I_k^2 R_k. \quad (1)$$

Here,  $I_k$  and  $R_k$  are the current and resistance of coil  $k$  respectively.  $k = 1, 2, 3$  where 1 is the inner most nested coil.  $\alpha$  = the number of nested coils.

### B. The Bitter Plate

In order to accurately estimate the power produced by the magnet, an expression for the electrical resistance of the magnet must be derived, which begins with defining a single conducting plate. The conducting plate is assumed to be that of an annulus ignoring cooling hole geometry for simplicity and not the actual Bitter Arc used in the magnet, as seen in Fig. 2. The following derivations for a Bitter annulus follow a sequence leading to the calculation of the magnet's resistance and other important relationships that help with progressing the optimized magnet design.

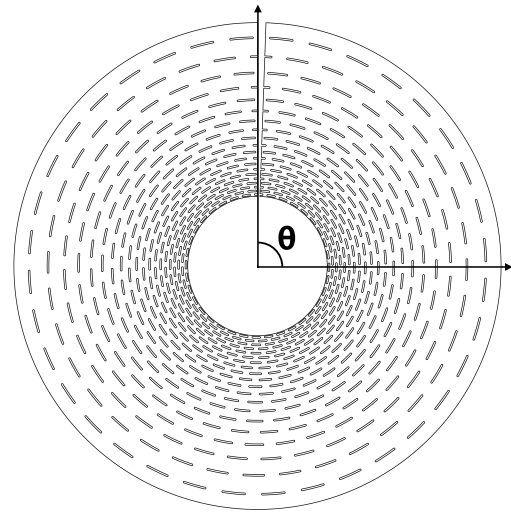


Fig. 2. Conducting Bitter Arc with elongated cooling holes.

### 1) Electric Potential

To find the electric potential of the Bitter annulus we use a set of boundary conditions that at  $\theta = 0$  there is some electric potential  $\phi = V_0$  and the annulus is electrically grounded at  $\theta = 2\pi$ ,  $\phi = 0$ . The potential will only be a function of  $\theta$ . The solution to Laplace's equation in scalar cylindrical coordinates for the electric potential of a Bitter annulus yields:

$$\phi(\theta) = \frac{V_0}{2\pi}(2\pi - \theta). \quad (2)$$

### 2) Electric Field

The electric field of the Bitter annulus is equal to the negative gradient of the electric potential, where the only non-zero term is the theta component,

$$\mathbf{E}(r) = -\frac{1}{r} \frac{\partial \phi}{\partial \theta} \hat{\theta}. \quad (3)$$

Substituting Eqn. (2) into Eqn. (3) gives the electric field of the Bitter annulus:

$$\mathbf{E}(r) = \frac{1}{r} \frac{V_0}{2\pi} \hat{\theta}. \quad (4)$$

### 3) Current Density

Current density is given by Ohm's law, where  $\rho$  is resistivity. Using Eqn. (4) the current density becomes:

$$\mathbf{J}(r) = \frac{1}{\rho} \mathbf{E} = \frac{1}{\rho r} \frac{V_0}{2\pi} \hat{\theta}. \quad (5)$$

It can be seen that current density has a relationship that follows the inverse of the radius. Most of the ohmic heating produced by the coil will happen towards the inner radius. This is a key feature when prototyping the Bitter disk and is essential in designing the placement of the cooling holes.

### 4) Current

To find the total current, integrate Eqn. (5) over the cross-sectional area of the Bitter annulus,

$$I = \iint \mathbf{J} \cdot (\lambda dr dz \hat{\theta}). \quad (6)$$

A copper filling factor of the Bitter annulus,  $\lambda$ , accounts for the increase in resistance given by the cooling holes [9]. This factor can also be called space, packing, or density factor, and it is commonly used by designers to describe cooling hole density in Bitter magnets [10], [11]. For our case of optimization we will assume a constant filling factor throughout the nested coils, where  $\lambda$  will represent the ratio of the conductor's volume with cooling holes over the volume without cooling holes. Using Eqns. (5) and Eqn. (6) then integrating from 0 to the thickness of the bitter annulus,  $h$ , and from the inner radius,  $r_i$ , to the outer radius,  $r_o$ , results in the current flowing in the Bitter annulus:

$$I = \int_{r_i}^{r_o} \int_0^h \frac{V_0}{2\pi\rho} \frac{1}{r} \hat{\theta} \cdot (\lambda dz dr \hat{\theta}) = \frac{V_0 \lambda h}{2\pi\rho} \ln \frac{r_o}{r_i}. \quad (7)$$

### 5) Resistance

To find the resistance of the Bitter annulus we make use of Ohm's law once again. Substituting Eqn. (7) in for the current and simplifying:

$$R = \frac{V_0}{I} = \left( \frac{2\pi\rho}{\lambda h} \right) \frac{1}{\ln \frac{r_o}{r_i}}. \quad (8)$$

We now have a fully defined Bitter annulus that will help with formulating the optimization problem and provide quick results without the need of FEA.

### C. Coil Resistance

It is important to know the total resistance of the coil which will be substituted into Eqn. (1) and used as our objective function. There are three plate stacking methods that are common in Bitter-type magnet designs: continuous, helix and irregular stacking. The optimization will assume for continuous stacking. This stacking method was first used by Bitter and is still the most straightforward [12]. In this method, each conducting plate is assumed to be one turn of the magnet, which is the distance the current takes to complete a  $2\pi$  circle. The conductors are separated by an insulator of the same thickness and the current travels in a helix with the pitch equal to the thickness of the conductor.

Helix and irregular stacking methods involve a more complex design. Helix stacking uses multiple conductors to make up one magnetic turn. This method is employed to change the magnetic field density throughout the bore. It also reduces the mechanical and thermal stresses on the conductor, and allows for a thinner insulator to be used compared to the conductor's thickness. Irregular stacking is similar to but is an improvement to helix stacking where the only difference in stacking is the non-integer number of plates that make up a magnetic turn. In irregular stacking it is possible to change the magnetic turn thickness without increasing mechanical stresses [13].

Although it is assumed that the current makes a full magnetic turn in continuous stacking, however in practice that is not the case. There will be a cut of a certain degree made in order for the annulus to bend upwards to form a helix, as seen in Fig. 2. However, since the copper conductors are

stacked in series and resistance adds in series, we can closely approximate the resistance of the Type I and II coils as follows:

$$R_k = \left( N_k \frac{2\pi\rho}{\lambda_k h_k} \right) \frac{1}{\ln \frac{r_{ok}}{r_{ik}}}. \quad (9)$$

Here  $N_k$  is the total number of magnetic turns in the  $k^{th}$  coil as well as the total number of copper conductors in the coil.  $N_k$  can be modified to account for multiple conductors should the user decide to use helix stacking method. In Eqn. (9),  $\lambda_k$  now represents the copper filling factor of the entire coil, not just a single Bitter annulus.  $\rho$  is constant assuming that all coils are made of the same conducting material.

## III. MAGNETIC FIELD SOLVER OF NESTED MAGNET

A magnetic field solver is derived here for both Type I and II magnets. The magnetic field is used in the optimization to constraint the objective function. An assumption is first made to simplify the calculations, which is that each Bitter annulus is made of tightly-packed, thin conducting loops of wire. These wires are placed so that they fill the entire cross-section of a Bitter annulus neglecting cooling and fastener hole geometry. This allows thickness and radial current density of the conductor to be accounted for by the user defined number of wires in the cross-section. Illustrated in Fig. 3 is the general setup geometry of a Type I  $\alpha = 1$  magnet. The spacing,  $d_1$ , between the conductors at the center axes can easily be changed to simulate either a Type I or Type II magnet. Bitter Annuli after  $d_1$  are separated by the conductor's thickness to account for insulation. Insulation spacing and current density are two of the most important factors determining the magnetic field besides the inner radius and current magnitude. These are two features which make this magnetic field solver specialized to a continuously stacked Bitter coil.

### A. Magnetic Field Solver Setup

The magnetic field along the  $Z$  axis of a current carrying loop is derived from Biot-Savart's Law [14], [15]:

$$B_{wire} = \frac{\mu_0 I_c r^2}{2(r^2 + (z - \frac{d}{2})^2)^{\frac{3}{2}}}. \quad (10)$$

Here  $\mu_0$  represents the permeability of vacuum and  $z$  is the position on the  $Z$  axis;  $r$  is the placement of the wire on the  $R$  axis.  $d$  is the placement of the wire on the  $Z$  axis. The current,  $I_c$ , in each wire segment must also be defined. This is accomplished by taking the integrand from Eqn. (7) and discretizing the differentials,  $dz, dr \rightarrow \Delta z, \Delta r$ . The equation is then divided by the total number of wires radially,  $\eta_r$ , and axially,  $\eta_z$ . The conductor thickness,  $h$ , is replaced in terms of the geometric separation variables,  $h = (d_2 - d_1)/2$ . The resultant is current for each discrete wire as a function of radial location inside the cross section of a Bitter annulus is given by:

$$I_c = \frac{1}{\eta_r \eta_z} \frac{V_0 \lambda}{4\pi\rho r} (r_o - r_i)(d_2 - d_1). \quad (11)$$



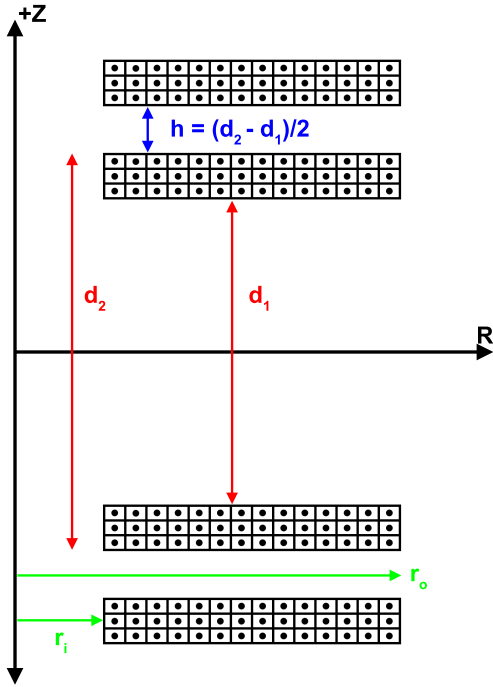


Fig. 3. Magnetic field solver geometry setup symmetric about the Z-axis for a Type I magnet, where  $\eta_r = 14$  and  $\eta_z = 3$ . The separation distance,  $d_1$ , is used to defined the two different Bitter magnet types. For Type I,  $d_1 \gg h$  and for Type II magnet,  $d_1 = h$ , where  $h$  is the annulus thickness.  $d_2$  is used to set the annulus thickness.

Substituting Eqn. (11) into Eqn. (10), represents the magnetic field of a wire inside a Bitter annulus as a function of both radial and axial position:

$$B_k[r, d] = \frac{V_{0k} \lambda \mu r}{2 \rho \pi \eta_r \eta_z} \frac{(d_{1k} - d_{2k})(r_{ik} - r_{ok})}{(4r^2 + (d - 2z)^2)^{3/2}}. \quad (12)$$

The magnetic field of the placed wire can be used to build a  $k^{\text{th}}$  Bitter magnet coil by the principle of superposition. An annulus is first put together by summing radially placed wires from  $r_i$  to  $r_o$  that differ in current from Eqn. (12), where  $(r_o - r_i)/\eta_r$  represents the distance between the wire segments radially. The annulus thickness is then created by summing over the variable  $d$ , where  $(d_2 - d_1)/\eta_z$  represents wire spacing axially. Next, two thick Bitter annuli separated by a distance of  $d_1$ , placed on positive and negative Z-axis as in Fig. 3, are superimposed. Lastly, the magnet is formed by superimposing the two thick annuli to have multiple instances of annuli symmetric about the R axis with  $(d_2 - d_1)/2$  spacing between sequential conductors. The result gives Z directional magnetic field for either Type I or II,  $k^{\text{th}}$  Bitter magnet coil:

$$B_{zk} = \sum_{i=0}^{N_k/2-1} \left[ \sum_{d_\gamma=0}^{\eta_z} \left( \sum_{r_\gamma=0}^{\eta_r} B_k[r, d_m] \right) + \dots \right. \\ \left. \sum_{d_\gamma=0}^{\eta_z} \left( \sum_{r_\gamma=0}^{\eta_r} B_k[r, d_n] \right) \right], \quad (13)$$

where:

$$r = r_{ik} + \left( \frac{r_{ok} - r_{ik}}{\eta_r} \right) r_\gamma, \\ d_m = d_{1k} + 2i(d_{2k} - d_{1k}) + \left( \frac{d_{2k} - d_{1k}}{2\eta_z} \right) d_\gamma, \\ d_n = -d_{2k} - 2i(d_{2k} - d_{1k}) + \left( \frac{d_{2k} - d_{1k}}{2\eta_z} \right) d_\gamma.$$

Here,  $i$ , is an iteration integer variable that represents an annulus at a certain position along the Z axis. The superposition of different annuli is dependent of  $d_1$  and  $d_2$ . At  $i = 0$  represents the first two annuli separated by a distance of  $d_1$  and given a thickness of  $(d_2 - d_1)/2$ . The resulting annuli after the first two at  $i = 0$  are spaced by the set conductor and insulator thickness. This is representative of a continuously stacked Bitter coil where the spacings represent the placement of insulators of same thickness of Bitter annuli. This also allows full control over  $d_1$  which is the defining characteristic between Type I and II magnets. For Type I magnet  $d_1 \gg$  annulus thickness and for Type II magnet  $d_1 =$  annulus thickness.

The use of a nested system will decrease the amount of power to be dissipated. The superposition of the B field from each coil  $k$ , given by Eqn. (13), represents a nested Bitter magnet system. The Z component magnetic field along the Z axis for a  $\alpha$  number of nested coils becomes:

$$\begin{aligned} \Omega=k \rightarrow \alpha \\ B_{IorII} [r_{i\Omega}, r_{o\Omega}, d_{1\Omega}, d_{2\Omega}, \lambda_\Omega, V_{0\Omega}, N_\Omega, z, \eta_r, \eta_z] = \\ \sum_{k=1}^{\alpha} B_{zk} \geq B_{GOAL}. \end{aligned} \quad (14)$$

By setting this equation equal to  $B_{GOAL} = 10T$  at  $z = 0$ , it will constrain our objective function to a domain where we can find design variables for optimization.

### B. Magnetic Field Solver Accuracy

To ensure that the magnetic field solver will give accurate results, the field at the axis of a long solenoid with filamentary current is computed and compared to the known solution for an ideal solenoid:

$$B_z = \mu_0 n I, \quad (15)$$

here  $I$  is the current and  $n$  is the turns per unit length. As a test case these parameters are arbitrarily set to  $I = 100A$ , and  $n = 500m^{-1}$  in Eqn. (15) resulting in a theoretical magnetic field of 0.0628T. In order to mimic the solenoid with the aforementioned parameters the magnetic field solver variables must then equal:  $\lambda = 1$ ,  $V_0 = 1.0608V$ ,  $N = 10,000$ ,  $r_i = 0.1m$ ,  $r_o = 0.101m$ ,  $d_1 = 0.001m$ ,  $d_2 = 0.003m$ . These variables are set to model 1mm by 1mm wires spaced 1mm apart. At  $\eta_r = \eta_z = 1000$  wire resolution yields a magnetic field of 0.0629T. The percent difference between the magnetic field solver and theoretical solution for these parameters is 0.195%.

The percent difference and computation times for varying number of edge wire elements of same aspect ratio,  $\eta_r = \eta_z$ , can be found in Fig. 4. As the total number of wire elements is increased the accuracy and computation time of the solver increases.

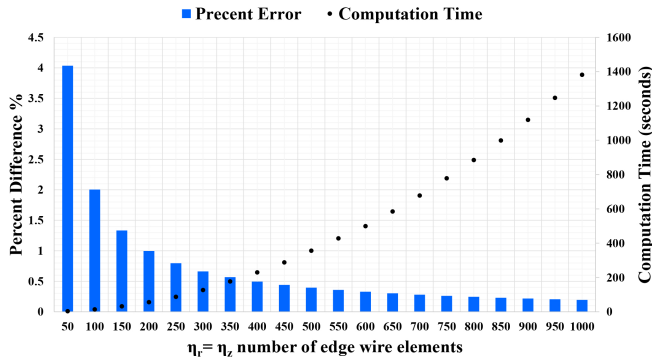


Fig. 4. The percent difference between the computed magnetic field of the solver and analytical solution of a long solenoid vs the number of edge wire elements for  $\eta_r$  and  $\eta_z$  of same aspect ratio. The solenoid model has the parameters:  $\lambda = 1$ ,  $V_0 = 1.0608\text{V}$ ,  $n = 500\text{m}^{-1}$ ,  $r_i = 0.1\text{m}$ ,  $r_o = 0.101\text{m}$ ,  $d_1 = 0.001\text{m}$ ,  $d_2 = 0.003\text{m}$ .

#### IV. OPTIMIZATION

High currents are associated with high magnetic fields, therefore optimization must be used to seek the lowest power possible to drive the coil at  $B_{GOAL}$ , while maximizing safety and minimizing cost. The objective of this optimization is to find the global minimum power output of a nested coil system by finding the optimum set of design variables. This optimization formulation will help determine whether or not it is feasible to dissipate enough power for safe operating conditions. Optimizations have been explored and solved with the Broyden Fletcher Goldfarb Shanno (BFGS) quasi-Newton method for multi-coil resistive magnet with high power densities [16]. Lagrangian finite element methods have also been developed to be used in optimal electromagnet designs [17]. Used here is a genetic algorithm implemented with MATLAB for magnets of relatively low power densities, for rapid preliminary designing [18], [19].

Type I and II magnets both with spanning  $\alpha$  values from 1 to 4 make up a total of 8 optimization cases to be analyzed. After all optimization cases are explored, we compare the  $\alpha$  values of each magnet type to determine which nested system would be most propitious. For this methodology, Type I and II magnets can be presented on a Pareto frontier where post optimization techniques can be used to make a final selection for the best magnet design [20]. Nested Bitter Magnet designs with smaller bore sizes than the one presented here will have more distinguishable Pareto frontiers between the total ohmic power output and the number of nested coils, making a nested design more appealing [21]. Furthermore, Type II magnets follow a similar decreasing ohmic power trend with an increasing  $\alpha$  number, but with much less magnitude than the Type I trend.

##### A. Formulation

The standard formulation of this optimization problem for both types of magnets is to minimize the electrical power

which drives the electromagnet:

$$\begin{aligned} & \min_{r_{i\Omega}, r_{o\Omega}, V_{0\Omega}, N_{\Omega}} \sum_{k=1}^{\alpha} \frac{(d_{2k} - d_{1k}) N_k V_{0k}^2 \lambda_k \ln \left[ \frac{r_{ok}}{r_{ik}} \right]}{4\pi\rho} \\ & \text{subject to} \\ (A) \quad & \begin{matrix} \Omega=k \rightarrow \alpha \\ B \\ I \text{ or II} \end{matrix} [r_{i\Omega}, r_{o\Omega}, d_{1\Omega}, d_{2\Omega}, \lambda_{\Omega}, \\ & \quad V_{0\Omega}, N_{\Omega}, 0, 50, 50] \geq B_{GOAL} \\ (B) \quad & \chi^L < \frac{B[z]}{B[z=0]} < \chi^U \\ (C) \quad & r_{min} < r_{ik} < r_{ok} \dots < r_{i\alpha} < r_{o\alpha} < r_{max} \\ (D) \quad & L_{min} < L_k, \dots, L_{\alpha} < L_{max} \\ (E) \quad & h_k, \dots, h_{\alpha} = \delta \\ (F) \quad & d_{split} < d_{1k}, \dots, d_{1\alpha} \\ (G) \quad & d_{1k}, \dots, d_{1\alpha} = h_k, \dots, h_{\alpha} = \delta \\ (H) \quad & N_k, \dots, N_{\alpha} > 0 \\ (I) \quad & V_{0k}, \dots, V_{0\alpha} > 0 \end{aligned}$$

The problem can be classified as a nonlinear constrained global optimization problem. We seek to minimize power by methodically finding solutions to both Type I and II magnet's design variables in the feasible space. The design space can be changed to create different sized magnets for different applications. However, this problem has a strict feasible space where the design variables enter into a seesaw type argument i.e. decreasing one variable leads to the increasing a different one. All design variables must also be constrained to realistic non-negative values.

##### B. Design Constraints

The corresponding equations will consist of both functional and geometric constraints.

###### 1) Constraint A

The magnitude of the magnetic field in the center of the experimental volume,  $z = 0$ , is the main functional constraint. This bounds the values of the current and impacts the objective function remarkably. Here  $B_{GOAL}$  is set to equal 10T.  $\eta_r$  and  $\eta_z$  are set to 50 and 50 respectively. The higher value of  $\eta$  the more wires fill the cross-section of the Bitter Conductor making the magnetic solver more accurate. These  $\eta$  values are chosen because it provides fast computation, on the order of milliseconds, and reasonable accuracy of the magnetic field. Increasing the value of  $\eta$  by a factor of 10 will increase the computation time of the magnetic solver to seconds and has a dramatic effect on the computation time of the optimization solver, on the order of hours.

###### 2) Constraint B

This inequality constraint serves as a percentage variance of the B field of either type magnet some distance away from the center on the  $z$  axis. It serves to constrain a highly uniform field in the experimental volume. A uniform field is needed for the experiments and for this case study we set 90% and 110% as the lower and upper limits respectively at  $z = 0.076\text{m}$  (3"), considered an acceptable deviation in the experimental requirements.

### 3) Constraint C

We impose a geometric inequality constraint for the inner and outer radii of the coils. This constraint confirms a nested magnet system. For a Type I magnet,  $r_{min}$  is set to be smaller than the radius of the vacuum chamber since the experimental volume can be accessed from the side of the magnet as seen in Fig. 1. We set this  $r_{min}$  for a Type I magnet to 0.0254m (1"). For a Type II magnet, the bore of our magnet,  $r_{min}$ , must be greater than or equal to the radius of the vacuum chamber. In our case we choose to set  $r_{min}$  to 0.08m (3.15").  $r_{max}$  is user defined, and is set to 0.2794m (11") for both magnet types.

To satisfy this constraint and improve computation time the radial position variables of nested coils can be removed and replaced with one variable for all nested cases called the tightness factor,  $b$ , from a stretching function. These types of functions are used for grid generation in FEA where the grid is concentrated towards a boundary [22]. The optimization makes use of the hyperbolic tangent stretching function proposed by Vinokur in 1983:

$$S(\zeta) = dr \left[ 1 + \frac{\tanh(b(\zeta - 1))}{\tanh(b)} \right], \quad (16)$$

where  $0 \leq \zeta \leq 1$  is the intermediate parametric space,  $S$  is the physical space,  $dr$  is the total radial extent of the nested magnet, and  $0 \leq b$  is the tightness factor. The parametric space is divided by the total number of radii in the current nested case which provides parametric coordinates to output the physical space of the radial positions. Therefore all radii for nested coil cases of both Type I and II are determined by the tightness factor. An increasing tightness factor will push the radii towards  $r_{min}$ , and a tightness factor of 0 will evenly displace all radii. In order to use the stretching function the outer radius of the preceding magnet coil must be equal to the inner radius of the following coil.

### 4) Constraint D

This inequality geometric constraint sets not the total length of the magnet, but just the length of one coil. Both types of magnets are symmetric about the center axes and from the magnetic field derivation we include the thickness of the insulator, thus the total magnet length of Type I and II  $k^{th}$  coils with insulation is as follows:

$$L_k = d_{1k} + 2N_k \left( \frac{d_{2k} - d_{1k}}{2} \right) - \left( \frac{d_{2k} - d_{1k}}{2} \right). \quad (17)$$

We set the minimum length of the coil,  $L_{min}$  to 0.127m (5") and the max,  $L_{max}$ , to 1m (39.3701") for both cases.

### 5) Constraint E

Plate thickness is a constraint that greatly affects the resistance and strength of the magnet. In the continuous stacking method our conducting plate thickness is:

$$h_k = \frac{d_{2k} - d_{1k}}{2}. \quad (18)$$

The material under consideration is a copper alloy because of its high tensile strength and low resistivity. For prototyping we are using standard copper, therefore a realistic margin is set to an integer amount of known manufactured sheet thicknesses. The optimization is constrained to copper conductor thicknesses from an array,  $\delta$ , with varying commercial values.

Thicknesses considered are: 0.00051m, 0.00064m, 0.00081m, 0.00102m, 0.00127m. Values below 0.00051m (0.02") are considered a foil for standard copper, which would not stand the Lorentz forces unless the copper is an alloy [23]. The conductor thickness,  $h$ , and the variable  $d_{1k}$ , sets the constant  $d_{2k}$ .

### 6) Constraint F (Type I Only)

The separation distance,  $d_{1k}$ , of the coils allows the conversion between a Type I and Type II. The minimum split separation distance for a Type I magnet,  $d_{split}$ , is set to the thickness of the proposed vacuum chamber, 0.1524m (6"). The optimization will always approach an answer close or equal to  $d_{split}$ . This is because the magnitude of the magnetic field can be maintained at lower currents as  $d_{1k}$  approaches zero.

### 7) Constraint G (Type II Only)

For Type II magnets,  $d_{1k}$ , is equal to the conductor's thickness,  $h_k$ , and is constrained to the array  $\delta$ .

### 8) Constraint H

The number of magnetic turns must be a non-negative value, and we predict a domain in which we believe the optimum value will fall under. As a result, the code only searches in integer numbers which cuts down on computing time. We use a domain for  $N_k$  of [100, 1000] turns.

### 9) Constraint I

Voltage per conductor is constrained to non-negative values and again we predict a domain that is realistic and based on experimental hardware available. To drive the magnet for 10 seconds there will be a power system consisting of a bank of capacitors or batteries. We set a domain of [0, 3] Volts for  $V_{ok}$ , the voltage per conducting plate. To find the total voltage drop per coil we use the following equation:

$$V_k = V_{ok} N_k. \quad (19)$$

To find the current load of the coil, important characteristic needed to design the power bank, Eqn. (7) is used.

## C. Design Parameters

There are several design parameters that results from this optimization. The copper filling factor,  $\lambda_k$ , is one of the most important parameters for the cooling methodology and is significant in the objective function. We use a value of 86% which is higher than other reported copper filling factors such as 77% [9], [24]. We will be operating at higher currents therefore a slightly high factor will help lowering the resistance. Most copper filling factors seem to fall in this range however, it is the choice of the designer to pick an adequate value.

Resistivity of the conducting material is another design parameter that plays an important role in minimization. The most notable alloy standard among high field Bitter magnets is CuAg [25]. This alloy has one of the highest ultimate tensile strengths compared to other alloys such as CuBe, Glidcop, CuZr, and ETP (Electrolytic Tough Pitch) Cu [26]. For our purposes we will assume the resistivity of ETP copper for prototyping and implementing the code.

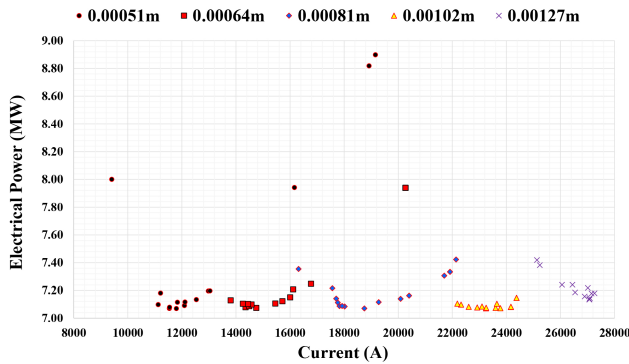


Fig. 5. Genetic algorithm solutions for a Type II,  $\alpha = 1$ , magnet of integer conductor thickness. Plotted is the objective function, electrical power, vs. the calculated current from the output variables

#### D. Genetic Algorithm Solver

To numerically obtain solutions a genetic algorithm (GA) is utilized. With a high number of constraints a direct search method is preferred rather than a gradient-based method. While this direct search method will converge to a solution slowly, it is less likely to fall subject to the noise of the constraints and converge to no solution. Finding a global optimum can be very difficult and this algorithm does not guarantee a global minimum.

GA is based on natural selection and is used to solve highly complex problems [27]. The flow of the algorithm consists of creating an initial population, with each individual having a fitness function (objective function) value evaluated at a set of variables. A random number generator is used to choose individuals from that generation to be the parents that produce the next generation. The children are determined by crossover and mutation rules, two main characteristics of GA. Crossover is the act of combining the parents' variables to form children and mutation is the random changes of the parents' variables to produce the child's variables. With many generations the solution should evolve to the most optimal case.

There are 8 optimization cases, each of which will be executed 75 times. Each execution produces an optimal solution found when either the function tolerance is below  $10^{-6}$  or the maximum generations of the GA have been achieved. The max generations of the GA are prescribed to equal the total design variables multiplied by 100. Each case has a different number of design variables to be optimized, determined by  $b$ ,  $V_{0\Omega}$ , and  $N_{\Omega}$ . Total executions of each case and the max generations per execution are user defined. GA is a stochastic solver and relies on the default MATLAB pseudorandom number stream to produce results [19]. A new number stream is produced with each execution; it is not user defined here because GA benefits from randomness. However, the state is saved for reproducibility. For this study the optimization runs a total of 600 different times. Each case must be executed more than once because the optimal solutions found by GA have a high probability to be local minima due to highly nonlinear objective function and constraints. While 75 executions is appropriate for our study, more can be conducted to minimize potential outliers. Fig. 5 shows 75 optimal GA-produced

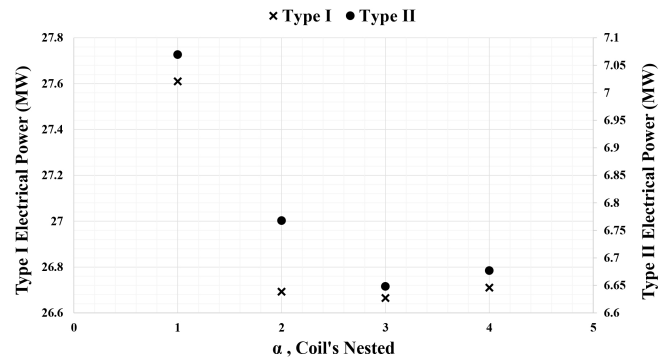


Fig. 6. Power output vs the number of coils nested,  $\alpha$ , for most optimum Type I and II magnets solutions

solutions, 15 each per conductor thickness, for the case of a Type II  $\alpha = 1$  magnet. The solutions remain clustered with respect to conductor thickness. The optimization may have not found the global optimum but with confidence it can be assumed that it falls in or near the cluster. The most suitable and realistic solution from the list is chosen by the user depending on experimental constraints such as current ratings on electronics. We search for solutions that evenly distribute current between nested coils, although this may result in a higher power output compared to other solutions.

#### V. OPTIMIZATION RESULTS

The most optimum solution for each magnet design case can be found in Fig. 6. Type I and II magnets have a Pareto frontier, characteristic of a nested system. We seek a solution that is both minimal in electrical power and the number of coils nested. A Pareto multi-objective optimization program has been formulated in MATLAB using a weighted mini-max technique to help select a solution from the optimal nested case [20], [28]. This post-process method takes the solutions of the main optimization (Electrical Power vs.  $\alpha$ ) if they have a Pareto frontier and finds the closest solution to the utopia point.

As  $\alpha$  increases for a Type I magnet we see a decrease in the electrical power. As the number of nested coils increases, the current can be distributed over the increasing coils, minimizing the power. Since the outer radius is bounded as  $\alpha$  continuously increases, the configuration will tend to a filamentary spool with multiple layers. Cooling a magnet of that design with such high currents is impractical, which is the underlying reason behind Francis Bitter's development of the water cooling magnet concept. The engineering complexity increases with  $\alpha$ , therefore it is not viable to construct a high  $\alpha$  magnet. The most optimum design of a Type I magnet under the presented conditions selected with the Pareto multi-objective post-process is an  $\alpha = 3$  magnet with a total power of 26.66 MW. A Type I magnet at these conditions is not feasible to be constructed for this dusty plasma experiment.

In Fig. 6, it is clear that a Type II magnet has a more optimum answer when compared to the Type I magnet. However, planned experiments include many optical measurements in which gaining optical access to our vacuum chamber is more

Type II Magnet	Optimization	Post-Optimization
$\alpha = 1$	$\eta_r = 50$ $\eta_z = 50$	$\eta_r = 1000$ $\eta_z = 1000$
Total Power	7.15 MW	7.73 MW
Resistance	27.9 m $\Omega$	27.9 m $\Omega$
Total Voltage Drop	446.72 V	464.92 V
$V_1$	2.45 V	2.55 V
$I_1$	16.005 kA	16.634 kA
$N_1$	182	182
$L_1$	232.96 mm	232.96 mm
$h_1$	0.64 mm	0.64 mm
$r_{i1}$	80 mm	80 mm
$r_{o1}$	279.4 mm	279.4 mm

TABLE I: The elected preliminary magnet design parameters from optimization and post-optimization.

challenging. The optimization points follow a similar trend but less magnitude than the Type I magnet. The most optimum value for a Type II magnet will be  $\alpha = 3$  with a power output of 6.65 MW. The constraints on the magnets bore for Type II is confined to a larger value than is normally seen in many Bitter magnets. Therefore, a significant decrease in electrical power as the nested coils increase is not observed hence providing no engineering benefit of a nested Type II magnet.

Due to Type I magnet's split distance and Type II magnet's bore size constraints for dusty plasma experiments, the benefits of a nested system disappear. The solutions to the Type II  $\alpha = 1$  magnet have been elected for preliminary designing. A magnet's design parameters are chosen from the generated optimization solutions as seen in Fig. 5. The solution selected is not the most optimal but is the most achievable in terms of experimental equipment. Table I summarizes the initial design parameters of the magnet from the selected solution. While these initial design parameters satisfy constraint A, they only do so for lower magnetic field solver resolutions ( $\eta_r = 50$  and  $\eta_z = 50$ ). In order to reach 10T, the design parameters must be input back into the magnetic field solver at higher resolution,  $\eta_r = 1000$  and  $\eta_z = 1000$ , such that the voltage increases to achieve the desired 10T magnetic field. This post-process will increase the amount of electrical power but must be used because running the optimization at high resolution is not practical. These post-optimization design parameters are summarized in Table I as well.

This magnitude of power puts substantial requirements on heat removal and mechanical stresses. Therefore, using these results, feasibility of the system can now be assessed in terms of cooling need and mechanical strength. Thermal feasibility is determined by analytical optimum placement of the cooling holes and minimum required flow rate [29]. The magnet is then modeled in CAD and evaluated in ANSYS Maxwell to solve for the magnetic force. The forces output from Maxwell into ANSYS WorkBench where they are imported into ANSYS Static Structural to test for mechanical stress feasibility. If any feasible criteria requirements are not met, the optimization process must start over with relaxed constraints on the magnetic field optimization.

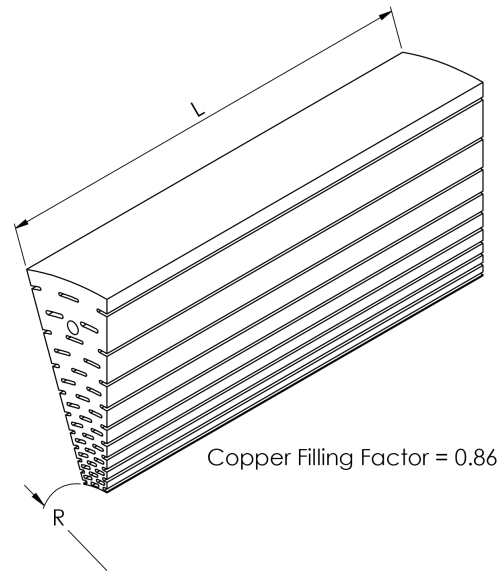


Fig. 7. FEA model (A): a 20° cross section of a CAD modeled Type II magnet with copper filling factor of 0.86 with cooling hole geometry.

## VI. OPTIMIZATION RESULTS VS FINITE ELEMENT ANALYSIS RESULTS

The optimal design variables from Table I are used to make two different FEA models—one with a cooling hole geometry (A) and one model without a cooling hole geometry (B)—to conduct magnetostatic analyses. The magnetic field along the Z-axis from the bore's center ( $z = 0$ ) out to 500mm of both FEA models are compared to the optimization's magnetic field solver results from Table I. The magnetic field solver can best account for the cooling hole geometry by introducing the copper filling factor analytically into Eqn. (6). Unlike the FEA Model (A), the solver cannot physically model the cooling hole geometry. For the FEA model (A), a 20° cross section of the case study magnet, seen in Fig. 7, is designed in CAD and then applied with a current-turn excitation in ANSYS Maxwell to the boundary faces. The total length of the magnet is cut in half and a symmetric boundary condition is used to decrease the computational time. The process is similar for the FEA model (B), however no cooling hole geometries are modeled. Copper's conductivity of this model is multiplied by the copper filling factor to account for the cooling holes without actually modeling them, just like the magnetic field solver. In Fig. 8, the magnitude of the magnetic field along the Z-axis of the FEA models and magnetic field solver are plotted. At the very center of the bore 10T, 9.60T and 9.95T are achieved with the magnetic field solver, FEA model (A), and FEA model (B) respectively. There is a 4% averaged difference between the magnetic field solver and FEA model (A) along the axis. The percentage difference is the effect of the cooling and tiered hole geometry on current density throughout the conductor as seen in Fig. 9. The current density goes to zero inside cooling hole geometry where the magnetic field solver does not. Keeping all parameters constant in FEA model (A) and the solver, the same drop in magnetic field is seen for varying



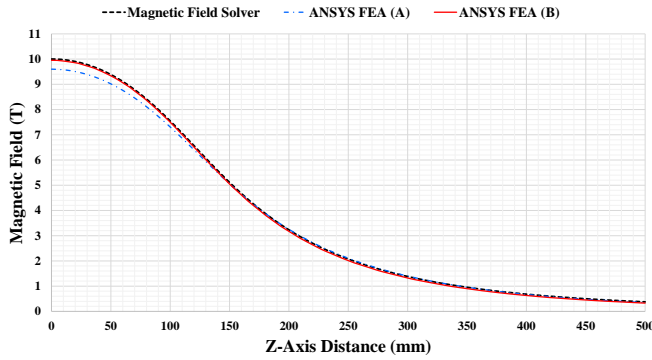


Fig. 8. Comparison of magnetic field solver with  $\eta_r = \eta_z = 1000$  against FEA model (A), modeling cooling hole geometry, and FEA model (B), neglecting cooling hole geometry.

currents. The geometry of the cooling holes is the source of field drop and is a benefit that can be modeled with FEA. The averaged percent difference between the magnetic field solver and FEA model (B) is 0.5%. Since FEA model (B) accurately represents the geometry of the magnetic field solver, higher  $\eta_r$  and  $\eta_z$  resolution in the solver will converge to the FEA model (B) solution as shown in section III-B.

Fig. 9 shows the FEA calculated current density profile along the radius at a certain degree,  $r$ , on the conductor. This figure also shows the theoretical current density which can be recast in terms of the total current by inserting the resistance of the Bitter annulus, Eqn. (8), into Ohm's law and solving for voltage,

$$V_0 = IR = \frac{I}{\ln \frac{r_o}{r_i}} \frac{2\pi}{\sigma \lambda h}, \quad (20)$$

and inserting into Eqn. (5), current density becomes

$$\mathbf{J}(r) = \frac{I}{\lambda h r \ln \frac{r_o}{r_i}} \hat{\theta}. \quad (21)$$

The two profiles, Eqn. (21) and FEA model, follow a very similar curve, which follows the relationship of the inverse of the conductor's radius. Between each cooling hole, the magnitude of the current density is higher than the theoretical curve, which is also the case for the segment near the tierod support hole. The circular geometry of both the tierod support and elongated cooling holes adds an increased amount of current density.

Fig. 10 shows the FEA model (A) magnetic field profile, strongest in the bore of the magnet, even with the cooling hole geometry. The magnetic field solver code over-predicts the magnitude of the magnetic field of the FEA analysis, but the difference narrows when higher values of  $\eta$  are used. This optimization method has been used to design and construct a 1 Tesla Type II Bitter prototype magnet [30]. Experimental results from the prototype magnet will be used to verify and validate the optimization method presented in this paper.

## VII. CONCLUSION

The magnetic solver presented here is a faster method to calculate the magnet field on axis of Type I and II Bitter magnets compared to an FEA analysis. This analytical method

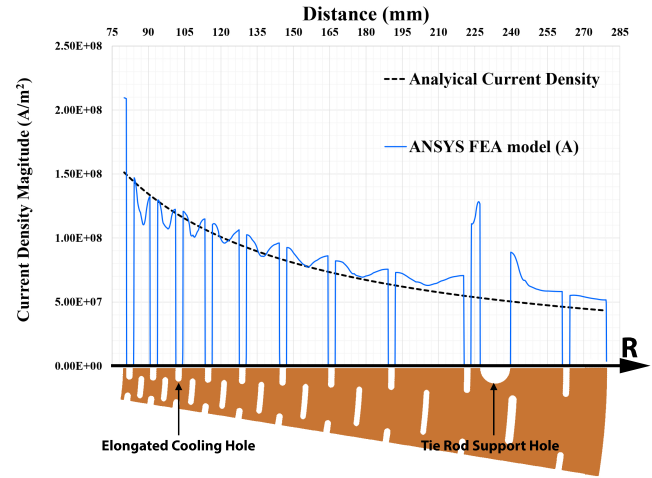


Fig. 9. Current density of Bitter magnet FEA model (A) with parameters from Table I along radius  $R$ . The cooling hole geometry drops the current density which yields lower magnetic fields within the bore.

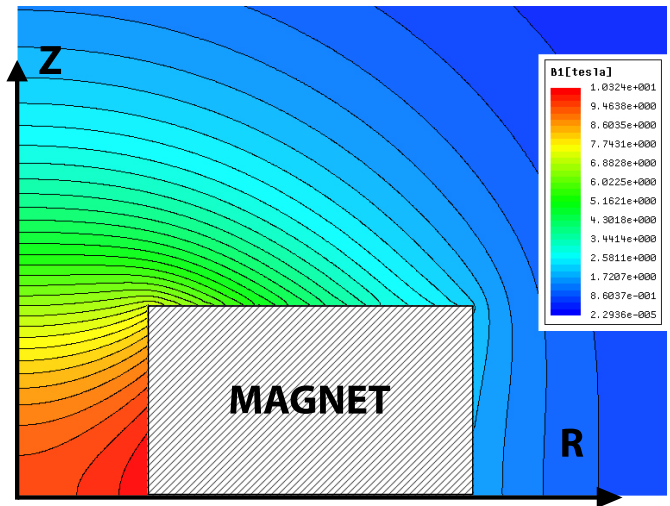


Fig. 10. The contour plot of magnetic field for elected preliminary symmetric Bitter magnet FEA model (A) with the bore located parallel to the  $Z$  axis.

is beneficial to the user, as no complicated external CAD models need to be developed, and a user can test preliminary designs varying many of the important features. With a minimal difference from the FEA results, the magnetic solver is a good representation of the magnetic field to be used as a main constraint in the optimization solver. The optimization solver is robust and can be easily modified for more constraints or algorithm options, however not all optimization problems can be solved. Provided that  $\alpha$  remains small, it can be concluded that the optimization methodology presented here is both a simple and acceptable mean of approximation in delivering a procedure for a low powered Bitter magnet design configuration.

The optimization code leads to a foundational design driven by user-defined constraints. These initiatory design values can be advantageous to thermal assessments for ideal placement of water cooling holes. Furthermore, these values are also appropriate for mechanical stress investigations for ultimate

placement of the tierod holes. This initial design method can be used as a tool for early magnet design concepts and will prove useful from an engineering perspective on cost analysis and administering initial bill of materials. Through the optimization, a Type II magnet is the best fit for future dusty plasma research and experimentation. FEA models verify that the optimization results predict the realistic model. Construction of a 1/10th magnetic field prototype Type II magnet and its subsystems is in progress and will be used to verify the large scale version outlined in Table I. Electromagnets such as these require optimization to ensure safety, efficiency, and reliability.

## ACKNOWLEDGMENTS

We would like to acknowledge the Special Research Assistantship/Initiative Support and the Department of Mechanical Engineering at UMBC for supporting this research.

## REFERENCES

- [1] C. A. Romero-Talamas, E. Bates, W. Birmingham, and W. Rivera, "DPLX: Experiment to Investigate Heating and Stability in Magnetized Rotating Dusty Plasmas," *IEEE Trans. Plasma Sci.*, vol. 44, no. 4, pp. 535–539, 2015.
- [2] E. Thomas, R. Merlino, and M. Rosenberg, "Magnetized Dusty plasmas: the next frontier for complex plasma research," *Plasma Phys. Control. Fusion*, vol. 54, no. 12, p. 124034, 2006.
- [3] F. Bitter, "The Design of powerful electromagnets part II. The magnetizing coil," *Rev. Sci. Instrum.*, vol. 7, pp. 482–8, 1936.
- [4] M. Bird, S. Bole, Y. Eyssa, B. Gao, and H. Schneider-Muntau, "Design of a Poly-Bitter Magnet at NHMFL," *IEEE Trans. Magn.*, vol. 32, no. 4, pp. 2542–2545, 1996.
- [5] S. Wieggers, J. Rook, A. Ouden, J. Perenboom, and J. Mann, "Design and Construction of a 38 T Resistive Magnet at the Nijmegen High Field Magnet Laboratory," *IEEE Trans. Appl. Supercond.*, vol. 22, no. 3, 2012.
- [6] B. Gao, H. Schneider-Muntau, Y. Eyssa, and M. Bird, "A new concept in Bitter disk design," *IEEE Trans. Magn.*, vol. 32, no. 4, pp. 2503–6, 1996.
- [7] H. Schneider-Muntau, J. Toth, and H. Weijers, "Generation of the Highest Continuous Magnetic Fields," *IEEE Trans. Appl. Supercond.*, vol. 14, no. 2, 2004.
- [8] M. Bird, I. Dixon, and J. Toth, "Design of the Next Generation of Florida-Bitter Magnets at the NHMFL," *IEEE Trans. Appl. Supercond.*, vol. 14, no. 2, pp. 1253–1256, 2004.
- [9] D. Sabulsky, C. Parker, N. Gemelke, and C. Chin, "Efficient continuous-duty Bitter-type electromagnets for cold atom experiments," *Rev. Sci. Instrum.*, vol. 84, p. 104706, 2013.
- [10] M. Bird, "Resistive magnet technology for hybrid inserts," *Supercond. Sci. Technol.*, vol. 17, pp. R19–R–33, 2004.
- [11] Y. Nakagawa, "A design of high-power water-cooled magnet suitable for hybrid magnet," *IEEE Trans. Magn.*, vol. 17, no. 5, pp. 1786–1789, 1981.
- [12] F. Bitter, "The design of powerful electromagnets part IV. the new magnet laboratory at M.I.T." *Rev. Sci. Instrum.*, vol. 10, pp. 373–381, 1939.
- [13] J. Chen and M. D. Bird, "Resistive Solenoid Development at the NHMFL Based on Irregular Stacking Method," *IEEE Trans. Appl. Supercond.*, vol. 22, no. 3, 2012.
- [14] D. J. Griffiths, *Introduction to electrodynamics*, 3rd ed. Upper Saddle River, N.J.: Prentice Hall, 1999, p.p. 202-242.
- [15] W. R. Smythe, *static and dynamic electricity*, 3rd ed. New York: McGraw-Hill, 1967, chapter 7.
- [16] S. Prestemon, P. Gilmore, B. J. Gao, and M. D. Bird, "Design optimization of multi-coil resistive magnets," *IEEE Trans. Magn.*, vol. 32, no. 4, pp. 2550–2553, 1996.
- [17] A. Marrocco and O. Pironneau, "Optimum Design with Lagrangian Finite Elements: Design of an Electromagnet," *Comput. Methods in Appl. Mech. Eng.*, vol. 15, no. 3, pp. 277–308, 1978.
- [18] C. Reeves and J. Rowe, *Genetic Algorithms Principles and Perspectives*. Boston: Kluwer Academic Publishers, 2003, p.p. 180-213.
- [19] M. Inc., "Global optimization toolbox," 2016.
- [20] K. M. Miettinen, *Nonlinear Multiobjective optimization*. Boston: Kluwer Academic Publishers, 1999, p.p. 5-33.
- [21] D. Scap, M. Hoić, and A. Jokzć, "Determination of the pareto frontier for multi-objective optimization problem," *Trans. FAMENA*, vol. 37, no. 2, pp. 15–28, 2013.
- [22] V. Lisejkin, *Grid generation methods*. Berlin: Springer, 1999, p.p. 101-130.
- [23] J. Wood, J. Embury, and M. Ashby, "An approach to materials processing and selection for high-field magnet design," *ACTA MATER*, vol. 45, no. 3, pp. 1099–1104, 1996.
- [24] T. Luan, T. Zhou, X. Chen, and Z. Ma, "A modified bitter-type electromagnet and control system for cold atom experiments," *Rev. Sci. Instrum.*, vol. 85, p. 024701, 2014.
- [25] Y. Sakai, K. Inoue, and H. Maeda, "High-Strength and High-Conductivity Cu-Ag Alloy Sheets: New Promising Conductor for High-Field Bitter Coils," *IEEE Trans. Magn.*, vol. 30, no. 4, pp. 2114–2117, 1994.
- [26] R. Weggel, J. Ratka, W. Spiegelberg, and Y. Sakai, "Strength of Hycon 3 HP Be-Cu and other copper alloys from 20C to 200C," *IEEE Trans. Magn.*, vol. 30, no. 4, pp. 2188–2191, 1994.
- [27] J. Holland, "Genetic Algorithms," *Sci Am*, vol. 267, no. 1, p. 055701, 1992.
- [28] G. Mastinu and M. Gobbi, *Optimal design of complex mechanical systems with applications to vehicle engineering*. Berlin: Springer, 2006, p.p. 40-90.
- [29] W. J. Birmingham, E. M. Bates, and C. A. Romero-Talamas, "Analytic Thermal Design of Bitter-Type Solenoids," *J Therm Sci Eng Appl*, vol. 8, no. 2, p. 021008, 2015.
- [30] E. Bates, W. Birmingham, and C. A. Romero-Talamas, "Development of a Bitter-Type Magnet System," *IEEE Trans. Plasma Sci.*, vol. 44, no. 4, pp. 540–544, 2015.